

Millimeter-wave spectroscopy of the $^{13}\text{CH}_3\text{OD}$ isotopic species of methyl alcohol

Li-Hong Xu^a, R.M. Lees^{a*}, O. Zakharenko^b, H.S.P. Müller^b, F. Lewen^b, S. Schlemmer^b, K.M. Menten^c

^a*Centre for Laser, Atomic and Molecular Physics (CLAMS), Department of Physics, University of New Brunswick, 100 Tucker Park Road, Saint John, NB, Canada E2L 4L5*

^b*I. Physikalisches Institut, Universität zu Köln, 50937 Köln, Germany*

^c*Max-Planck-Institut für Radioastronomie, 53121 Bonn, Germany*

Abstract

The dramatic increase in sensitivity, spectral coverage and resolution of radio astronomical facilities in recent years has opened new possibilities for observation of chemical differentiation and isotopic fractionation in protostellar sources to shed light on their spatial and temporal evolution. In warm interstellar environments, methanol is an abundant species, hence spectral data for its isotopic forms are of special interest. In the present work, the millimeter-wave spectrum of the $^{13}\text{CH}_3\text{OD}$ isotopologue has been investigated over the region from 150-510 GHz to provide a set of transition frequencies for potential astronomical application. The focus is on two types of prominent $^{13}\text{CH}_3\text{OD}$ spectral groupings, namely the *a*-type qR -branch multiplets and the *b*-type Q -branches. Line positions are reported for the $^qR(J)$ clusters for $J = 3$ to 10 for the $v_t = 0$ and 1 torsional states, and for a number of $v_t = 0$ and 1 $^rQ(J)$ or $^pQ(J)$ line series up to $J = 25$. The frequencies have been fitted to a multi-parameter torsion-rotation Hamiltonian, and upper level excitation energies have been calculated from the resulting molecular constants.

1. Introduction

The dramatic advances in sensitivity, detector bandwidth and resolution of radio astronomical facilities in recent years have greatly enhanced the study of the intricate molecular environments in star-forming regions [1]. Numerous detailed astronomical surveys are highlighting the importance of the physics and chemistry of the protostellar stages, with observations of chemical differentiation and isotopic fractionation shedding new light on the spatial and temporal evolution and the physical conditions of the warm and dense environments of newly formed stars [1-7].

Since its discovery in the interstellar medium 50 years ago [8], methanol has been an important species in astronomical studies of interstellar clouds and star-forming regions, with its rich spectrum providing a valuable probe into the thermal and spatial structures of the sources [9]. As the high abundance of methanol renders numerous lines of the main $^{12}\text{CH}_3^{16}\text{OH}$ species optically thick in many sources, the C-13, O-18 and deuterated isotopologues have also been important in permitting observations deep into the source regions in order to obtain more accurate determinations of column densities (molecules per cm^2) and abundance profiles as well as information on astrochemical processes [1,2,4-7,9,10]. While the terrestrial and general cosmic abundance of deuterium is very low, much higher D/H ratios can be observed ranging up to several percent in warm protostellar regions with active chemistry [1,2,4-7,10,11]. Thus, the

importance of deuterated isotopologues is significantly enhanced, providing motivation for the present study of $^{13}\text{CH}_3\text{OD}$.

The only previous spectroscopic data for $^{13}\text{CH}_3\text{OD}$ are from the investigation of the fundamental $J = 1 \leftarrow 0$ *a*-type qR_0 transitions of numerous methanol isotopic species by Venkateswarlu et al. [12]. This study provided effective *B* rotational constants for the *A* and *E* torsional symmetry species for the $v_t = 0$ to 2 torsional states. In the present work, we have extended observation and analysis to the $^qR_K(J)$ multiplets from $J = 3$ to 10 and $K = 0$ to 10 for the $v_t = 0, 1$ ground and first excited torsional states, and have also explored the *b*-type $^rQ(J)$ and $^pQ(J)$ $v_t = 0$ and $v_t = 1$ *Q*-branches lying in the spectral region from 150 to 510 GHz. Both types of spectral feature have characteristic “fingerprint” structures, giving a dataset with optimum possibility for astronomical detection. The data have been analyzed with a multi-parameter global fitting program, thereby providing upper-state excitation energies and a set of molecular constants that is compared to those for related isotopic species.

2. Experimental Details

Measurements over the 150 to 510 GHz millimeter-wave (MMW) region were carried out on the Cologne MMW spectrometer, details of which have been reported previously [13,14]. The MMW radiation was generated by a sequence of frequency multipliers (Virginia Diodes) driven by a MW synthesizer locked to an atomic clock. Schottky detectors were employed, with lock-in amplification in $2f$ mode. The free-space absorption cell was a 5-m Pyrex tube, double-passed via a roof-top reflector, with a Teflon Brewster window at the entrance to the cell to separate the incident and reflected beams.

The $^{13}\text{CH}_3\text{OD}$ sample was produced by taking advantage of both the rapid D/H exchange at the hydroxyl group known for methanol and the strong methanol propensity for adsorption on cell surfaces. Prior to the start of the $^{13}\text{CH}_3\text{OD}$ study, an investigation of the $^{12}\text{CH}_3\text{OD}$ isotopologue had been ongoing in the 350–510 GHz region and served to precondition the cell walls. A sample of $^{13}\text{CH}_3\text{OH}$ was then mixed with an equal volume of D_2O and the cell was filled with the vapour to a pressure of approximately 20 μbar . An initial sweep from 395–400 GHz showed a mixture of isotopologues, with strong $^{12}\text{CH}_3\text{OD}$ and $^{12}\text{CH}_3\text{OH}$ lines of comparable intensity together with weak $^{13}\text{CH}_3\text{OD}$ and $^{13}\text{CH}_3\text{OH}$ features down by about an order of magnitude. As we continued to higher frequencies with numerous sample refill cycles, however, the $^{12}\text{CH}_3\text{OD}$ was gradually replaced on the cell walls and pumped out, and the $^{13}\text{CH}_3\text{OD}$ lines became strongly dominant in the spectrum. We repeated the initial 395–400 GHz sweep a few days later, and the previous $^{12}\text{CH}_3\text{OD}$ and $^{12}\text{CH}_3\text{OH}$ features now had very low intensity.

For the majority of the multi-GHz sweeps, the step size between spectral points was set to 108 kHz. The JPL SMAP analysis program [15] was used for peak-fitting, but in some later cases the peak centres were interpolated directly from the point listings for convenience. In general, the accuracy of the line positions is estimated conservatively to be within ± 0.05 MHz.

3. Spectral structure and notation

The only lines previously known for $^{13}\text{CH}_3\text{OD}$ were the $J_K = 1_0 \leftarrow 0_0$ *A/E* doublets for the $v_t = 0$ to 2 torsional states [12], which provided effective *B*-values. Thus, to guide the initial search,

values for the other major torsion-rotation parameters were estimated from those of the related $^{12}\text{CH}_3\text{OH}$, $^{12}\text{CH}_3\text{OD}$ and $^{13}\text{CH}_3\text{OH}$ species [16-18]. The spectral features could then be predicted employing a modified version of the BELGI program used for energy calculation and global fitting [16,19]. It was decided initially to target *a*-type *R*-branch multiplets and *b*-type *Q* branches, two classes of features that form distinctive line groupings in the spectrum [9] that would have the highest likelihood for successful astronomical detection. Both involve relatively close sets of transitions covering a broad range of excitation energy, providing distinctive fingerprints for identification as well as sensitivity to the physical conditions of an astronomical source.

In simplest form, the ground-state molecular torsion-rotation energies can be written as

$$E_{t-r}(v_t, TS, J, K) = E_t(v_t, TS, K) + B_{\text{eff}}J(J+1) + (A - B)_{\text{eff}}K^2 + \text{higher-order terms} \quad (1)$$

where E_t is the (K -dependent) torsional energy, B_{eff} and $(A - B)_{\text{eff}}$ are effective rotational constants, J is the overall rotational angular momentum with component K along the molecular *a*-axis, v_t is the torsional quantum number and $TS = A$ or E denotes the torsional symmetry. For $|K| > 0$ for E levels, a signed K will be used with $K > 0$ and $K < 0$ levels forming different classes, while the A levels with $K > 0$ are split by molecular asymmetry into K -doublets with the components distinguished as A^+ or A^- . The higher-order terms include centrifugal distortion, J -dependent asymmetry shifts and torsion-rotation interactions.

Transitions induced by the μ_a component of the molecular dipole moment have a $\Delta K = 0$ selection rule, whereas those induced by μ_b normally follow the rule $\Delta K = \pm 1$. Both types have $\Delta J = 0, \pm 1$ selection rules, denoted as *P*, *Q* or *R* for $\Delta J = -1, 0$ or $+1$, respectively. An initial p, q or r prefix is also used similarly to indicate ΔK , giving the convenient notation ${}^qR_K(J)$ for a $(J+1)_K \leftarrow J_K$ *a*-type *R*-branch transition and ${}^pQ_K(J)$ or ${}^rQ_K(J)$ for $J_{K-1} \leftarrow J_K$ or $J_{K+1} \leftarrow J_K$ *Q*-branch transitions.

For an *a*-type *R*-branch transition with $\Delta K = 0$ and $\Delta J = +1$, the basic frequency from Eq. (1) is independent of K , TS and v_t and is given simply as:

$${}^qR(J) = 2B_{\text{eff}}(J+1) \quad (2)$$

The higher-order terms then broaden this into a series of tight v_t -multiplets shifting down with increasing v_t , each containing $2(2J+1)$ transitions of differing K and TS . Fig. 1 shows the $^{13}\text{CH}_3\text{OD}$ ${}^qR(8)$ *a*-type multiplets for $v_t = 0$ and $v_t = 1$, illustrating the close clustering in the spectrum. With A and E lines from $K = 0$ to 8, each v_t -multiplet contains 34 transitions with upper level excitation energies ranging from 66 to 255 cm^{-1} for $v_t = 0$ and 242 to 457 cm^{-1} for $v_t = 1$.

For a $K+1 \leftarrow K$ *Q*-branch, the ${}^rQ_K(J)$ members would all coincide in lowest order (as for a rigid symmetric-top molecule), but the higher-order terms introduce shifts strongly dependent on J . Thus, the typical *Q* branch appears as a series of lines closely spaced near the origin and then gradually spreading as J increases [7], as shown in Fig. 2 for the $K = -2 \leftarrow -1$ E $v_t = 0$ *Q*-branch. Three lines also appear in Fig. 2 from the $K = 2A^+ \leftarrow 1A^-$ $v_t = 0$ *Q*-branch that initially moves to low frequency but turns around at $J = 19$ and returns due to the differing J -dependence of the K -

doubling for $K = 1$ and $K = 2$. The $K = -3 \leftarrow -2 E v_t = 0 Q$ -branch is illustrated in Fig. 3, initially shading to lower frequency, coming to a head at $Q11$, and then reversing due to competition among the different higher-order contributions as J rises. (Note that the branch origin in the inset is at the upper limit of our spectral region where the MMW power is dropping off rapidly, so is rather difficult to see.)

4. Measurements

From the spectral predictions, we could select scan regions likely to contain significant $^{13}\text{CH}_3\text{OD}$ R -branch and/or Q -branch structures. Then, by comparing a template of the expected transition positions against the plotted spectra, we could search for those features via pattern recognition. An early success was the scan from 395-400 GHz in Fig. 1, in which the clear line clusters corresponding to the $v_t = 0$ and $1^qR(8)$ R -branch multiplets are seen as well as several lines of the $K = 3 \leftarrow 2 E v_t = 0 Q$ -branch. The latter were within a few MHz of the predicted positions, hence we then proceeded to track the full Q -branch with short targeted individual 108 MHz scans for each line from the origin up to $J = 25$. As new assignments were made, they were then incorporated into the input dataset for the global fitting program in order to refine the molecular parameters and the predictions in an iterative cycle.

Proceeding in this way with a combination of broad multi-GHz scans plus targeted short scans for individual Q -branch lines and updating the predictions as we went, we were able to assign and measure all of the A and E ${}^qR_K(J)$ transitions from $J = 3$ to 10 with $K = 0$ to 10 for both $v_t = 0$ and 1, as well as 7 Q branches for each of the $v_t = 0$ and 1 torsional states. Tables 1 and 2 list the R -branch transitions for $v_t = 0$ and $v_t = 1$, respectively, giving line positions, (o – c) residuals, upper level excitation energies for the transitions and relative intensity factors. Here the lines are ordered successively by J , torsional symmetry and then K , but a line list in increasing frequency order is also provided in the supplementary material. For the Q branches, we tracked all lines within our observational range of 150-510 GHz up to a maximum J of 25. The results are presented in Tables 3 and 4 for $v_t = 0$ and $v_t = 1$, respectively, ordered by torsional symmetry, K and then J .

For the $v_t = 0 E$ levels from $K = 0$ to 2, as seen previously for $^{12}\text{CH}_3\text{OD}$ [17] and $^{12}\text{CD}_3\text{OD}$ [20], the well-known K -labeling difficulties [17,19-23] arose in attaching appropriate K values to the computed energies to ensure that they met the intuitively reasonable criterion of following smooth trajectories with increasing J with no level crossings or sudden jumps. The problem is illustrated here in Fig. 4 for the J -reduced energies given by $[E_{t-r} - 0.738J(J+1)]$ where 0.736 cm^{-1} is the effective B -value, showing several distinct anomalies in the K -labels assigned by the computer. (A similar problem occurs for $v_t = 1$ also where the computer has the $-2 E$ curve coming down and crossing the $-1 E$ curve between $J = 23$ and 24.) The issue is due primarily to the off-diagonal $\Delta K = \pm 1$ and $\Delta K = \pm 2$ asymmetry elements in the torsion-rotation matrix that couple the basis states to give K -mixed eigenfunctions. As these elements are strongly J -dependent, the mixing increases rapidly with J and can lead to a change in K -character that triggers the computer K -labeling algorithm to suddenly switch between curves. In the spectrum, these alterations in K -character can modify the effective selection rules for affected transition

series, resulting in significant changes in the intensity patterns. This is seen for example in Table 4 in the sharp reduction of the computed transition strengths for the $K = -2 \leftarrow -3 E v_t=1 Q$ branch as it evolves towards a “forbidden” $K = -1 \leftarrow -3$ series at high J due to the $\{-1/-2\} E$ mixing.

In the present work, we have manually rearranged the K -labelling, using Excel spreadsheet difference tables and charts to ensure smooth, non-crossing behavior for all substates as shown in Fig. 5, with correspondingly smooth J -progressions for all sub-band frequencies. The resulting table of adjusted energy levels is included in the supplementary material. However, a problem still remains for the spectral fitting in that the input data must be labelled in conformity with the computer’s choice of K -values, otherwise large ($o - c$) residuals will result that can derail the fit [17]. The major issue here was the slow avoided crossing of the $K = 0$ and $-1 E v_t = 0$ levels around $J = 17$. This presented some difficulty to the energy calculation program, which output identical energies for the two $J = 17$ levels (an impossibility) and interchanged the two states for $J > 17$. This impacted our original measurements, because in following the computer K -labeling above $J = 17$ for the “ $K = -2 \leftarrow -1$ ” $E v_t = 0 Q$ -branch we were actually tracking lines of the $K = -2 \leftarrow 0 E Q$ -branch that appears due to intensity borrowing induced by the asymmetry mixing. Subsequently, from the spreadsheet smoothing, we could deduce the missing $J = 17 K = 0 E$ energy, and then sort out and locate the further lines of the $K = -2 \leftarrow -1$ and $-2 \leftarrow 0 E v_t = 0 Q$ -branches that are given in Table 3.

Valuable confirmation of the R -branch and lower- J Q -branch assignments was provided from closed combination loops of transitions, as illustrated in Fig. 6. The net change in energy going around a 4-sided loop should be zero, and, as shown in the figure caption, our observed loop defects are indeed close to zero to well within experimental uncertainty. For each of the reported Q branches, this check was carried out for all possible loops containing R -branch partners within our observed range from $R(3)$ to $R(10)$ in order to confirm the assignments.

5. Spectral fitting and molecular parameters

In order to obtain molecular constants for $^{13}\text{CH}_3\text{OD}$, the $v_t = 0$ and $v_t = 1$ transition frequencies in Tables 1 to 4 plus the original $J = 1_0 \leftarrow 0_0$ lines from [12] were fitted employing a slightly modified version of the BELGI torsion-rotation program [16,19]. In lowest order, the basic form for the torsional energy of Eq.(1) in the RAM axis system used is

$$E_t = F \langle P_\gamma + \rho P_a \rangle^2 + V_3/2 \langle 1 - \cos 3\gamma \rangle \quad (3)$$

where F is the internal rotation constant, P_γ is the angular momentum of the methyl top, V_3 is the height of the torsional potential barrier and γ is the angle of internal rotation. The parameter ρ accounts for the fraction of overall axial angular momentum K contributing to the top momentum, and acts as a scaling factor determining the period of oscillation of the torsional energies as a function of K . With incorporation of the molecular asymmetry term $(B - C)(P_b^2 - P_c^2)$ and the product of inertia term $D_{ab}(P_a P_b + P_b P_a)$ into Eq.(1), higher-order terms are then added to Eqs.(1) and (3) in power-series fashion as products of the torsional and rotational operators in successively higher order [16,19].

In total, 791 aR -branch and Q -branch frequencies were measured, including 74 unresolved A K -doublet transitions. In the absence of a feature to treat the latter as single blended lines, both K -doublet components were included separately in the fit. Then, with the exclusion of the lines indicated by asterisks in Tables 1 to 4 that were affected by doublet broadening, partially blended with close neighbors or showed anomalous intensity or large ($\sigma - c$) residuals, the final fit contained 779 transitions in all. The present observations were input with identical uncertainties, and the four early $1_0 \leftarrow 0_0$ lines were assigned uncertainties 10x greater. The final iteration of the fit incorporated 63 parameters and reproduced the data with an overall rms deviation of 0.101 MHz. The rms deviation for the $v_t = 0$ lines alone was 0.068 MHz, not far above the estimated experimental uncertainty of 0.05 MHz, while that for the weaker $v_t = 1$ lines was about twice as great at 0.125 MHz. The values obtained for the primary molecular constants are presented in Table 5, along with those of the related ${}^{12}\text{CH}_3\text{OD}$, ${}^{12}\text{CH}_3\text{OH}$ and ${}^{13}\text{CH}_3\text{OH}$ isotopologues. The ${}^{13}\text{CH}_3\text{OD}$ results are quite comparable to the ${}^{12}\text{CH}_3\text{OD}$ values, with small decreases in each term. A list of all the fitted ${}^{13}\text{CH}_3\text{OD}$ parameters is included in the supplementary material.

6. Conclusion

In this work, the MMW spectrum of the ${}^{13}\text{CH}_3\text{OD}$ isotopic species of methanol has been explored in the region from 150 to 510 GHz. The $R3$ to $R10$ multiplets of a -type aR -branch transitions together with a total of 7 b -type pQ and rQ branches have been identified and measured for each of the $v_t = 0$ and $v_t = 1$ torsional states. These are strong and relatively compact features with characteristic spectral patterns that should serve as a good dataset for potential detection in sensitive astronomical surveys of important protostellar sources. Observations in star-forming regions of the ${}^{13}\text{CH}_3\text{OD}$ isotopologue together with its ${}^{13}\text{CH}_3\text{OH}$ and ${}^{12}\text{CH}_3\text{OD}$ relatives could shed light on the source ${}^{13}\text{C}/{}^{12}\text{C}$ and D/H ratios and give a further window into the astrochemical processes and the temporal and spatial evolution of the sources.

The observed transition frequencies have been analyzed with a multi-parameter torsion-rotation global fitting program that reproduces the data to close to measurement uncertainty. A valuable set of calculated ground-state level energies has also thereby been obtained from the computer output. This will serve as a base for future extension of the assignments to b -type R -branch and P -branch transitions and possibly higher torsional levels to expand the dataset and give a comprehensive spectral picture of the ${}^{13}\text{CH}_3\text{OD}$ ground state.

Acknowledgments

R.M.L. and L.-H. Xu received financial support from the Natural Sciences and Engineering Research Council of Canada. R.M.L. expresses great appreciation for the warm hospitality and friendship extended to him and Li-Hong by Stephan and the whole Köln group during memorable visits. The work in Köln has been supported by the Deutsche Forschungsgemeinschaft (DFG) through the collaborative research grant SFB 956 (project ID 184018867), (sub-project B3), and through the Gerätezentrum "Cologne Center for Terahertz Spectroscopy" (project ID SCHL341/5-1).

References

- [1] J.K. Jørgensen, A. Belloche, R.T. Garrod, Astrochemistry During the Formation of Stars, *Annu. Rev. Astron. Astrophys.* 58 (2020) 727-778, and references therein, <https://doi.org/10.1146/annurev-astro-032620-021927>.
- [2] M.L. van Gelder, B. Tabone, L.Tychoniec, E.F. van Dishoeck, H. Beuther, A.C.A. Boogert, A. Caratti o Garatti, P.D. Klaassen, H. Linnartz, H.S.P. Müller, V. Taquet, Complex organic molecules in low-mass protostars on Solar System scales. I. Oxygen-bearing species, *Astron. Astrophys.* 639 (2020) A87, <https://doi.org/10.1051/0004-6361/202037758>.
- [3] A. Belloche, A. J. Maury, S. Maret, S. Anderl, A. Bacmann, Ph. André, S. Bontemps, S. Cabrit, C. Codella, M. Gaudel, F. Gueth, C. Lefèvre, B. Lefloch, L. Podio, L. Testi, Questioning the spatial origin of complex organic molecules in young protostars with the CALYPSO survey, *Astron. Astrophys.* 635 (2020) A198, <https://doi.org/10.1051/0004-6361/201937352>.
- [4] J.K. Jørgensen, H.S.P. Müller, H. Calcutt, A. Coutens, M.N. Drozdovskaya, K.I. Öberg, M.V. Persson, V. Taquet, E.F. van Dishoeck, S.F. Wampfler, The ALMA-PILS survey: isotopic composition of oxygen-containing complex organic molecules toward IRAS 16293-2422B, *Astron. Astrophys.* 620 (2018) A170, <https://doi.org/10.1051/0004-6361/201731667>.
- [5] J.K. Jørgensen, M.H.D. van der Wiel, A. Coutens, J.M. Lykke, H.S.P. Müller, E.F. van Dishoeck, H. Calcutt, P. Bjerkeli, T.L. Bourke, M.N. Drozdovskaya, C. Favre, E.C. Fayolle, R.T. Garrod, S.K. Jacobsen, K.I. Öberg, M.V. Persson, S.F. Wampfler, The ALMA Protostellar Interferometric Line Survey (PILS). First results from an unbiased submillimeter wavelength line survey of the Class 0 protostellar binary IRAS 16293-2422 with ALMA, *Astron. Astrophys.* 595 (2016) A117, <https://doi.org/10.1051/0004-6361/201628648>.
- [6] A. Belloche, H.S.P. Müller, R.T. Garrod, K.M. Menten, Exploring molecular complexity with ALMA (EMoCA): Deuterated complex organic molecules in Sagittarius B2(N2), *Astron. Astrophys.* 587 (2016) A91, <https://doi.org/10.1051/0004-6361/201527268>.
- [7] H.S.P. Müller, A. Belloche, Li-Hong Xu, R.M. Lees, R.T. Garrod, A. Walters, J. van Wijngaarden, F. Lewen, S. Schlemmer, K.M. Menten, , Exploring molecular complexity with ALMA (EMoCA): Alkanethiols and alkanols in Sagittarius B2(N2), *Astron. Astrophys.* 587 (2016) A92, <https://doi.org/10.1051/0004-6361/201527470>.
- [8] J.A. Ball, C.A. Gottlieb, A.E. Lilley, H.E. Radford, Detection of Methyl Alcohol in Sagittarius, *Astrophys. J. Lett.* 162 (1970) L203–L210, <https://doi.org/10.1086/180654>.
- [9] S. Wang et al., , Herschel observations of EXtra-Ordinary Sources (HEXOS): Methanol as a probe of physical conditions in Orion KL, *Astron. Astrophys.* 527 (2011) A95, <https://doi.org/10.1051/0004-6361/201015079>.
- [10] J.L. Neill, N.R. Crockett, E.A. Bergin, J.C. Pearson, Li-Hong Xu, Deuterated Molecules in Orion KL from Herschel/HIFI, *Astrophys. J.* 777 (2013) 85, <https://doi.org/10.1088/0004-637X/777/2/85>.
- [11] B. Parise, C. Ceccarelli, A.G.G.M. Tielens, A. Castets, E. Caux, B. Lefloch, S. Maret, Testing grain surface chemistry: a survey of deuterated formaldehyde and methanol in low-mass class 0 protostars, *Astron. Astrophys.* 453 (2006) 949–958, <https://doi.org/10.1051/0004-6361:20054476>.

- [12] P. Venkateswarlu, H.D. Edwards, W. Gordy, Methyl Alcohol. I. Microwave Spectrum, *J. Chem. Phys.* 23 (1955) 1195–1199, <https://doi.org/10.1063/1.1742239>.
- [13] J.-B. Bossa, M.H. Ordu, H.S.P. Müller, F. Lewen, S. Schlemmer, , Laboratory spectroscopy of 1,2-propanediol at millimeter and submillimeter wavelengths, *Astron. Astrophys.* 570 (2014) A12, <https://doi.org/10.1051/0004-6361/201424320>.
- [14] V.V. Ilyushin, O. Zakharenko, F. Lewen, S. Schlemmer, E.A. Alekseev, M. Pogrebnyak, R.M. Lees, Li-Hong Xu, A. Belloche, K.M. Menten, R.T. Garrod, H.S.P. Müller, Rotational spectrum of isotopic methyl mercaptan, $^{13}\text{CH}_3\text{SH}$, in the laboratory and towards Sagittarius B2(N2), *Can. J. Phys.* 98 (2020) 530–537, <https://doi.org/10.1139/cjp-2019-0421>.
- [15] See <http://spec.jpl.nasa.gov/ftp/pub/calpgm/SMAP/> for download of the SMAP spectral analysis program available from JPL.
- [16] Li-Hong Xu, J. Fisher, R. M. Lees, H.Y. Shi, J.T. Hougen, J.C. Pearson, B.J. Drouin, G. A. Blake, R. Braakman, Torsion rotation global analysis of the first three torsional states ($\nu = 0, 1, 2$) and terahertz database for methanol, *J. Mol. Spectrosc.* 251 (2008) 305–313, <https://doi.org/10.1016/j.jms.2008.03.017>.
- [17] M.S. Walsh, Li-Hong Xu, R.M. Lees, I. Mukhopadhyay, G. Moruzzi, B.P. Winnewisser, S. Albert, Rebecca A.H. Butler, F.C. DeLucia, Millimeter-Wave Spectra and Global Torsion-Rotation Analysis for the CH_3OD Isotopomer of Methanol, *J. Mol. Spectrosc.* 204 (2000) 60-71, <https://doi.org/10.1006/jmsp.2000.8201>.
- [18] Li-Hong Xu, R.M. Lees, Yun Hao, H.S.P. Müller, C.P. Endres, F. Lewen, S. Schlemmer, K.M. Menten, Millimeter wave and terahertz spectra and global fit of torsion-rotation transitions in the ground, first and second excited torsional states of $^{13}\text{CH}_3\text{OH}$ methanol, *J. Mol. Spectrosc.* 303 (2014) 1-7, <https://doi.org/10.1016/j.jms.2014.06.005>.
- [19] I. Kleiner, Asymmetric-top molecules containing one methyl-like internal rotor: Methods and codes for fitting and predicting spectra, *J. Mol. Spectrosc.* 260 (2010) 1–18, <https://doi.org/10.1016/j.jms.2009.12.011>.
- [20] L.-H. Xu, H.S.P. Müller, F.F.S. van der Tak, S. Thorwirth, The millimeter-wave spectrum of perdeuterated methanol, CD_3OD , *J. Mol. Spectrosc.* 228 (2004) 220–229, <https://doi.org/10.1016/j.jms.2004.04.015>.
- [21] J. Ortigoso, I. Kleiner, J.T. Hougen, The K -rotational labeling problem for eigenvectors from internal rotor calculations: Application to energy levels of acetaldehyde below the barrier, *J. Chem. Phys.* 110 (1999) 11688–10699, <https://doi.org/10.1063/1.479115>.
- [22] R.D. Suenram, G.Yu. Golubiatnikov, I. I. Leonov, J.T. Hougen, J. Ortigoso, I. Kleiner, G. T. Fraser, Reinvestigation of the Microwave Spectrum of Acetamide, *J. Mol. Spectrosc.* 208 (2001) 188–193, <https://doi.org/10.1006/jmsp.2001.8377>.
- [23] V. Ilyushin, A new scheme of K -labeling for torsion-rotation energy levels in low-barrier molecules, *J. Mol. Spectrosc.* 227 (2004) 140–150, <https://doi.org/10.1016/j.jms.2004.05.013>.
- [24] R.M. Lees, A Note on CH_3OD Spectra, Ground-State Energies and FIR Laser Assignments, *Int. J. Infrared Millimeter Waves* 21 (2000) 1787–1805, <https://doi.org/10.1023/A:1006727701859>.

List of Tables

Table 1

Millimeter-wave frequencies, upper level energies (E_u) and line strengths (μ^2S) for ${}^qR_K(J)$ *a*-type *R*-branch transitions in the $v_t = 0$ ground torsional state of ${}^{13}\text{CH}_3\text{OD}$

Table 2

Millimeter-wave frequencies, upper level energies (E_u) and line strengths (μ^2S) for ${}^qR_K(J)$ *a*-type *R*-branch transitions in the $v_t = 1$ first excited torsional state of ${}^{13}\text{CH}_3\text{OD}$

Table 3

Millimeter-wave frequencies, upper level energies (E_u) and line strengths (μ^2S) for ${}^rQ_K(J)$ and ${}^pQ_K(J)$ *b*-type *Q*-branch transitions in the $v_t = 0$ ground torsional state of ${}^{13}\text{CH}_3\text{OD}$

Table 4

Millimeter-wave frequencies, upper level energies (E_u) and line strengths (μ^2S) for ${}^rQ_K(J)$ and ${}^pQ_K(J)$ *b*-type *Q*-branch transitions in the $v_t = 1$ first excited torsional state of ${}^{13}\text{CH}_3\text{OD}$

Table 5

Principal fitted molecular parameters (in cm^{-1}) for ${}^{13}\text{CH}_3\text{OD}$ and comparison to related methanol isotopologues

List of Figures

Fig. 1. Section of the $^{13}\text{CH}_3\text{OD}$ MMW spectrum showing ${}^qR(8)$ a -type multiplets for $v_t = 0$ and $v_t = 1$.

Fig. 2. Section of the $^{13}\text{CH}_3\text{OD}$ MMW spectrum showing the origin of the $K = -2 \leftarrow -1 E$ $v_t = 0$ Q -branch from $J = 2$ to 7, along with several lines from the $K = 2A^+ \leftarrow 1A^-$ and $1A^- \leftarrow 0 A^+$ $v_t = 0$ Q -branches.

Fig. 3. Section of the $^{13}\text{CH}_3\text{OD}$ MMW spectrum showing the origin region for the $K = -3 \leftarrow -2 E$ $v_t = 0$ Q -branch from $J = 3$ to 14.

Fig. 4. J -reduced low- K $v_t = 0$ energy levels of E symmetry for $^{13}\text{CH}_3\text{OD}$, showing the original K -labeling assigned by the computer. Strong K -mixing at high J by asymmetry matrix elements leads to an apparent level crossing between the lower $K = 0E$ and $-1E$ states around $J = 17$ and sudden jumps in K -labelling along the $K = 0$ and ± 2 curves for $J > 25$.

Fig. 5. J -reduced low- K $v_t = 0$ energy levels of E symmetry for $^{13}\text{CH}_3\text{OD}$ with K -labeling empirically adjusted to remove the $K = 0E$ and $-1E$ level crossing at $J = 17$ and give smooth variation along all substate energy curves, analogous to the pattern for $^{12}\text{CH}_3\text{OD}$ [24].

Fig. 6. Combination loop diagram confirming assignments for $K = 2A$ and $3A$ R -branch and Q -branch $v_t = 0$ transitions of $^{13}\text{CH}_3\text{OD}$. Transition frequencies (in MHz) are: $a = 488126.413$, $b = 398547.526$, $c = 486693.816$, $d = 399980.113$, $e = 485840.596$, $f = 405794.833$, $g = 486582.463$, and $h = 405052.950$. Combination defect for loop A (blue solid arrows) is $\delta_A = a + b - c - d = 0.010$ MHz. Defect for loop B (red dotted arrows) is $\delta_B = e + f - g - h = 0.016$ MHz.

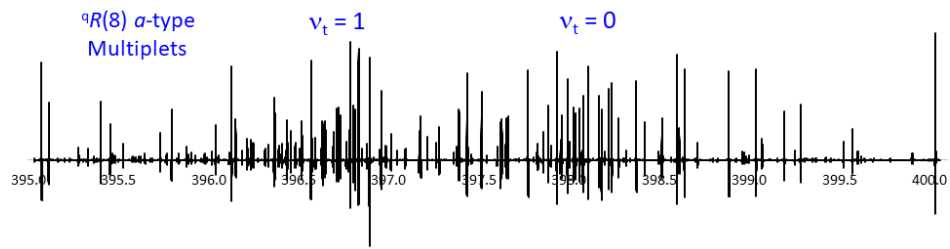


Fig. 1. Section of the $^{13}\text{CH}_3\text{OD}$ MMW spectrum showing ${}^qR(8)$ a -type multiplets for $v_t = 0$ and $v_t = 1$.

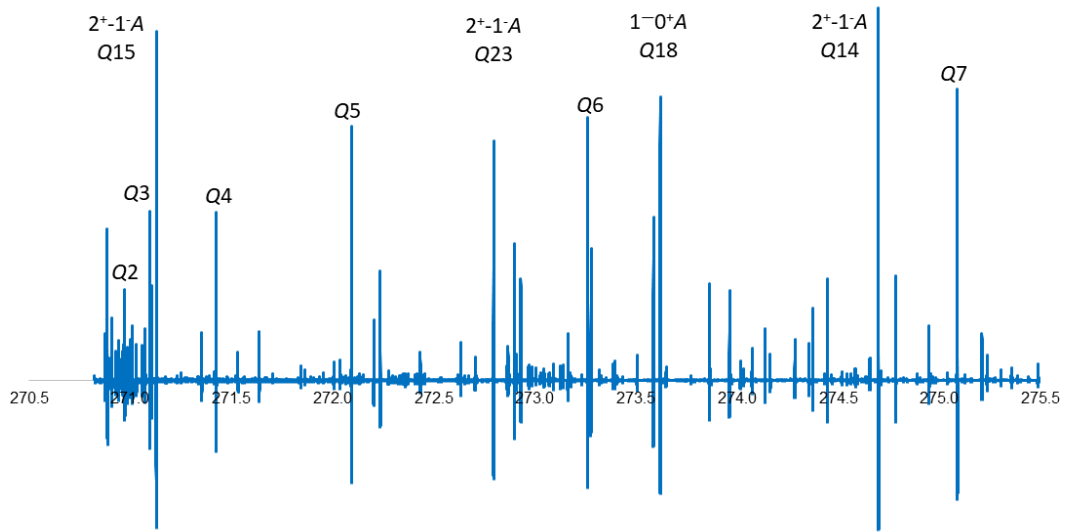


Fig. 2. Section of the $^{13}\text{CH}_3\text{OD}$ MMW spectrum showing the origin region of the $K = -2 \leftarrow -1 E$ $v_t = 0$ Q -branch from $J = 2$ to 7, along with several lines from the $K = 2A^+ \leftarrow 1A^-$ and $1A^- \leftarrow 0 A^+$ $v_t = 0$ Q -branches.

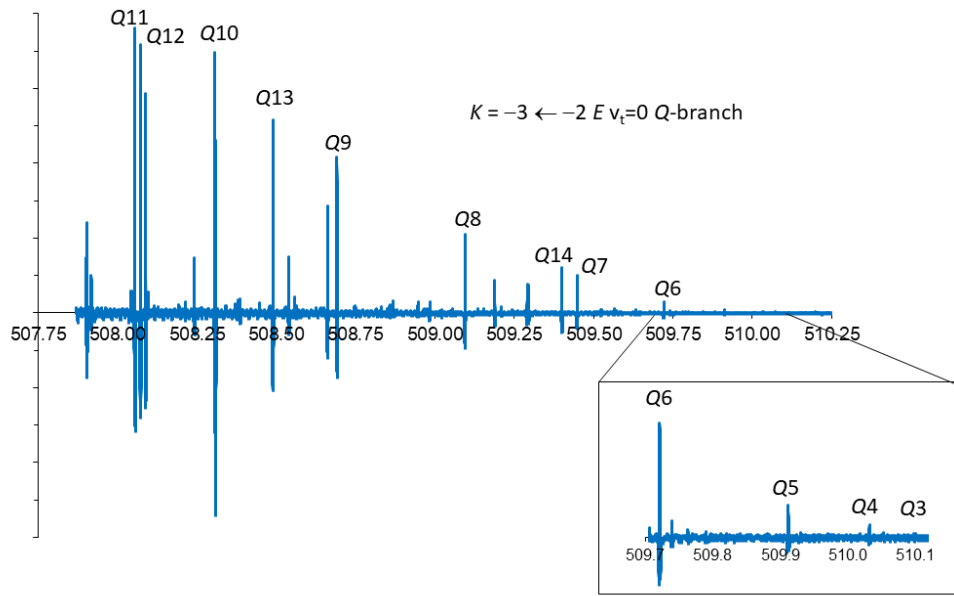


Fig. 3. Section of the $^{13}\text{CH}_3\text{OD}$ MMW spectrum showing the origin region for the $K = -3 \leftarrow -2$ $E v_t = 0$ Q-branch from $J = 3$ to 14.

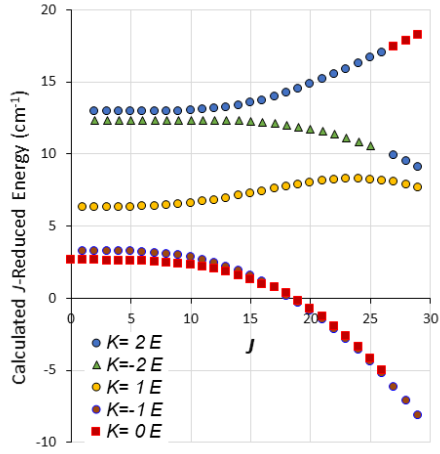


Fig. 4. J -reduced low- K $v_t = 0$ energy levels of E symmetry for $^{13}\text{CH}_3\text{OD}$, showing the original K -labeling assigned by the computer. Strong K -mixing at high J by asymmetry matrix elements leads to an apparent level crossing between the lower $K = 0E$ and $-1E$ states around $J = 17$ and sudden jumps in K -labelling along the $K = 0$ and ± 2 curves for $J > 25$.

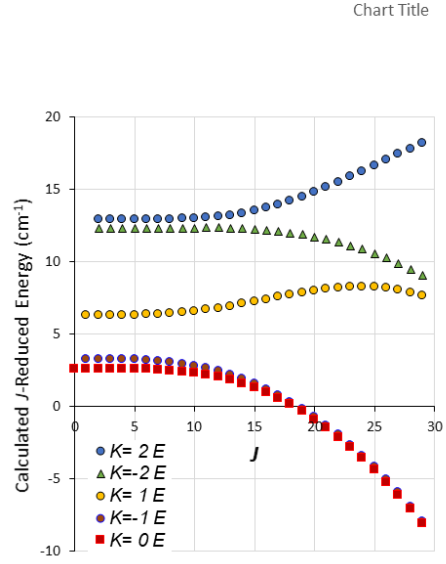


Fig. 5. J -reduced low- K $v_t = 0$ energy levels of E symmetry for $^{13}\text{CH}_3\text{OD}$ with K -labeling empirically adjusted to remove the $K = 0E$ and $-1E$ level crossing at $J = 17$ and give smooth variation along all substate energy curves, analogous to the pattern for $^{12}\text{CH}_3\text{OD}$ [24].

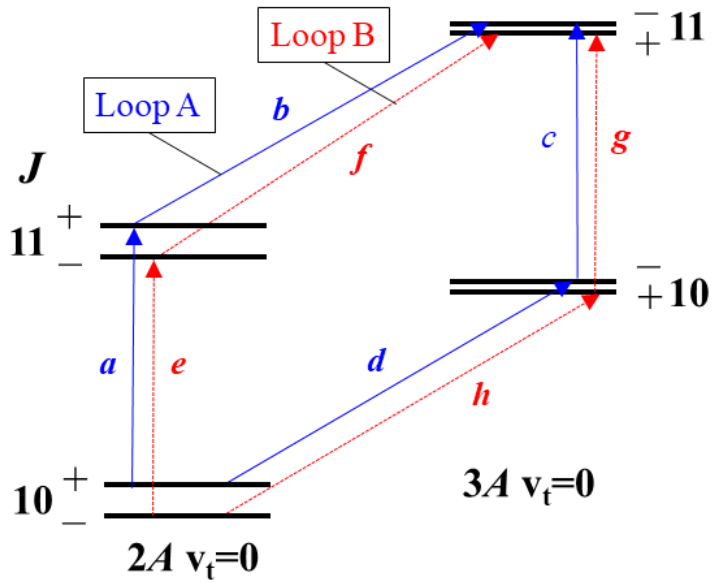


Fig. 6. Combination loop diagram confirming assignments for $K = 2A$ and $3A$ R -branch and Q -branch $v_t = 0$ transitions of $^{13}\text{CH}_3\text{OD}$. Transition frequencies (in MHz) are: $a = 488126.413$, $b = 398547.526$, $c = 486693.816$, $d = 399980.113$, $e = 485840.596$, $f = 405794.833$, $g = 486582.463$, and $h = 405052.950$. Combination defect for loop A (blue solid arrows) is $\delta_A = a + b - c - d = 0.010$ MHz. Defect for loop B (red dotted arrows) is $\delta_B = e + f - g - h = 0.016$ MHz.

Table 1

Millimeter-wave frequencies, upper level energies (E_u) and line strengths (μ^2S) for ${}^qR_K(J)$ a -type R -branch transitions in the $v_t = 0$ ground torsional state of ${}^{13}\text{CH}_3\text{OD}$

$J' - J''$	K	TS	v_{obs} (MHz)	(o-c) ^a	E_u (cm ⁻¹) ^a	μ^2S^c	$J' - J''$	K	TS	v_{obs} (MHz)	(o-c) ^a	E_u (cm ⁻¹) ^b	μ^2S^c
1 - 0	0	A+	44241.43 ^d	0.058	1.4757	0.68	7 - 6	0	A+	309036.218	0.032	41.2714	4.79
1 - 0	0	E	44228.26 ^d	0.045	4.0772	0.64	7 - 6	1	A+	304933.513	0.022	45.1596	4.68
4 - 3	0	A+	176848.386	0.019	14.7515	2.74	7 - 6	1	A-	313977.907	0.030	46.3676	4.67
4 - 3	1	A+	174337.152	0.019	18.9999	2.56	7 - 6	2	A+	310068.398	0.019	56.5624	4.33
4 - 3	1	A-	179514.003	0.032	19.4317	2.55	7 - 6	2	A-	309473.816	0.025	56.5177	4.33
4 - 3	2	A+	177028.294	0.012	29.9744	2.02	7 - 6	3	A+	309660.927	0.009	69.9871	3.84
4 - 3	2	A-	176921.667	0.012	29.9690	2.02	7 - 6	3	A-	309671.888	0.011	69.9877	3.84
4 - 3	3	A+	176949.01	0.049*	43.4263	1.18	7 - 6	4	A+	309658.654	-0.034	88.4201	3.21
4 - 3	3	A-	176949.43	-0.040*	43.4263	1.18	7 - 6	4	A-	309658.654	0.048	88.4201	3.21
4 - 3	0	E	176745.180	0.042	17.3465	2.56	7 - 6	5	A±	309612.249	0.014	115.5043	2.33
4 - 3	1	E	177173.969	0.020	21.0621	2.52	7 - 6	6	A±	309537.363	-0.047*	150.0557	0.92
4 - 3	2	E	177008.316	0.001	27.6732	2.03	7 - 6	0	E	308663.091	0.036	43.8399	4.46
4 - 3	3	E	176976.207	0.002	41.2089	1.19	7 - 6	1	E	310771.040	0.090	47.6983	4.61
4 - 3	-1	E	176696.221	-0.015	18.0005	2.54	7 - 6	2	E	309944.848	0.007	54.2528	4.35
4 - 3	-2	E	177024.867	0.018	27.0542	2.04	7 - 6	3	E	309758.081	0.004	67.7765	3.90
4 - 3	-3	E	176956.259	0.007	44.0671	1.18	7 - 6	4	E	309648.718	-0.005	90.1485	3.20
5 - 4	0	A+	220972.803	0.019	22.1223	3.42	7 - 6	5	E	309562.992	0.008	118.1565	2.30
5 - 4	1	A+	217890.551	0.010	26.2680	3.27	7 - 6	6	E	309519.739	-0.027	148.8213	1.25
5 - 4	1	A-	224359.449	0.019	26.9155	3.27	7 - 6	-1	E	308131.389	0.008	44.4603	4.62
5 - 4	2	A+	221338.029	-0.013	37.3574	2.83	7 - 6	-2	E	309960.163	0.022	53.6363	4.38
5 - 4	2	A-	221124.955	-0.001	37.3449	2.83	7 - 6	-3	E	309687.065	0.012	70.6297	3.86
5 - 4	3	A+	221186.650	0.028	50.8043	2.15	7 - 6	-4	E	309597.045	-0.009	91.4177	3.16
5 - 4	3	A-	221188.444	-0.006	50.8044	2.15	7 - 6	-5	E	309585.078	0.010	115.5173	2.32
5 - 4	4	A+	221185.629	-0.007	69.2375	1.22	7 - 6	-6	E	309567.818	-0.010	147.0827	1.26
5 - 4	4	A-	221185.629	-0.002	69.2375	1.22	8 - 7	0	A+	352953.588	0.041	53.0447	5.48
5 - 4	0	E	220805.854	0.041	24.7118	3.20	8 - 7	1	A+	348416.167	-0.008	56.7815	5.37
5 - 4	1	E	221615.720	0.023	28.4544	3.22	8 - 7	1	A-	358740.668	0.033	58.3339	5.37
5 - 4	2	E	221291.468	0.013	35.0547	2.84	8 - 7	2	A+	354501.246	-0.001	68.3873	5.05
5 - 4	3	E	221229.939	-0.012	48.5883	2.18	8 - 7	2	A-	353612.161	0.003	68.3129	5.05
5 - 4	4	E	221179.371	0.011	70.9665	1.22	8 - 7	3	A+	353896.360	0.047*	81.7918	4.62
5 - 4	-1	E	220649.514	-0.012	25.3605	3.25	8 - 7	3	A-	353918.231	0.019	81.7931	4.62
5 - 4	-2	E	221318.654	0.015	34.4366	2.86	8 - 7	4	A+	353894.679	-0.126*	100.2248	4.08
5 - 4	-3	E	221197.982	0.016	51.4454	2.16	8 - 7	4	A-	353894.679	0.100*	100.2248	4.08
5 - 4	-4	E	221151.955	-0.019	72.2386	1.21	8 - 7	5	A±	353835.193	0.009	127.3070	3.32
6 - 5	0	A+	265039.112	0.027	30.9631	4.11	8 - 7	6	A±	353741.895	0.003	161.8553	2.31
6 - 5	1	A+	261423.842	-0.002	34.9881	3.98	8 - 7	7	A±	353652.671	-0.090	199.7406	1.25
6 - 5	1	A-	269182.401	0.009	35.8945	3.97	8 - 7	0	E	352431.127	0.037	55.5957	5.08
6 - 5	2	A+	265682.610	0.009	46.2196	3.59	8 - 7	1	E	355479.651	0.018	59.5559	5.29
6 - 5	2	A-	265310.223	0.025	46.1947	3.59	8 - 7	2	E	354347.030	0.022	66.0725	5.07
6 - 5	3	A+	265424.121	0.012	59.6579	3.03	8 - 7	3	E	354035.028	0.012	79.5859	4.69
6 - 5	3	A-	265428.980	-0.002	59.6581	3.03	8 - 7	4	E	353882.510	-0.024	101.9528	4.07
6 - 5	4	A+	265422.282	-0.007	78.0910	2.27	8 - 7	5	E	353771.717	-0.043	129.9571	3.27
6 - 5	4	A-	265422.282	0.018	78.0910	2.27	8 - 7	6	E	353718.461	-0.055	160.6201	2.35
6 - 5	5	A±	265386.698	0.000	105.1768	1.25	8 - 7	7	E	353710.436	0.034*	196.9174	1.27
6 - 5	0	E	264783.542	0.055	33.5440	3.84	8 - 7	-1	E	351646.487	-0.006	56.1900	5.28
6 - 5	1	E	266146.936	0.040	37.3321	3.92	8 - 7	-2	E	354288.306	0.002	65.4541	5.10
6 - 5	2	E	265599.554	0.009	43.9141	3.61	8 - 7	-3	E	353935.142	-0.008	82.4357	4.64
6 - 5	3	E	265490.166	0.018	57.4441	3.07	8 - 7	-4	E	353813.979	-0.012	103.2196	4.02
6 - 5	4	E	265414.303	0.003	79.8197	2.26	8 - 7	-5	E	353798.492	-0.022	127.3188	3.30
6 - 5	5	E	265349.107	-0.020	107.8306	1.23	8 - 7	-6	E	353779.339	0.006	158.8835	2.38
6 - 5	-1	E	264465.447	0.000	34.1821	3.94	8 - 7	-7	E	353707.794	-0.058*	199.0790	1.27
6 - 5	-2	E	265632.138	0.016	43.2972	3.63	9 - 8	0	A+	396781.475	0.024	66.2799	6.16
6 - 5	-3	E	265441.453	0.006	60.2996	3.04	9 - 8	1	A+	391868.858	-0.011	69.8529	6.07
6 - 5	-4	E	265376.197	0.001	81.0906	2.23	9 - 8	1	A-	403465.121	0.018	71.7921	6.06
6 - 5	-5	E	265367.070	-0.005	105.1907	1.24	9 - 8	2	A+	398986.256	0.018	81.6960	5.76

Table 1 (continued)

$J' - J''$	K	TS	v_{obs} (MHz)	(o-c) ^a	E_u (cm ⁻¹) ^a	$\mu^2 S^c$	$J' - J''$	K	TS	v_{obs} (MHz)	(o-c) ^a	E_u (cm ⁻¹) ^b	$\mu^2 S^c$
9 - 8	2	A-	397721.769	0.020	81.5795	5.76	10 - 9	7	E	442086.589	0.001	224.9364	3.46
9 - 8	3	A+	398129.265	-0.021*	95.0719	5.38	10 - 9	8	E	442026.508	-0.026	270.0279	2.44
9 - 8	3	A-	398169.406	0.015	95.0746	5.38	10 - 9	9	E	441888.190	-0.294	322.0368	1.27
9 - 8	4	A+	398130.449	-0.181*	113.5050	4.91	10 - 9	-1	E	438282.382	0.011	83.9860	6.53
9 - 8	4	A-	398130.449	0.360*	113.5050	4.91	10 - 9	-2	E	442824.650	0.005	93.5207	6.51
9 - 8	5	A+	398055.143	-0.021	140.5847	4.23	10 - 9	-3	E	442440.387	-0.011	110.4760	6.15
9 - 8	5	A-	398055.143	-0.024	140.5847	4.23	10 - 9	-4	E	442233.883	-0.012	131.2477	5.63
9 - 8	6	A±	397940.236	-0.068	175.1291	3.36	10 - 9	-5	E	442209.165	-0.004	155.3454	5.07
9 - 8	7	A±	397833.665	-0.101	213.0110	2.37	10 - 9	-6	E	442186.696	-0.013	186.9087	4.36
9 - 8	8	A±	397805.194	0.094	254.7112	0.00	10 - 9	-7	E	442087.870	-0.036	227.0980	3.45
9 - 8	0	E	396076.694	0.041	68.8074	5.68	10 - 9	-8	E	441941.337	-0.271*	272.2938	2.40
9 - 8	1	E	400252.160	0.007	72.9068	5.98	10 - 9	-9	E	441853.781	0.131*	320.2916	1.27
9 - 8	2	E	398835.625	-0.006	79.3763	5.77	11 - 10	0	A+	484136.221	0.003	97.1228	7.53
9 - 8	3	E	398322.238	-0.004	92.8725	5.45	11 - 10	1	A+	478673.705	0.000	100.3394	7.46
9 - 8	4	E	398115.642	0.004	115.2325	4.90	11 - 10	1	A-	492775.053	0.015	103.1778	7.43
9 - 8	5	E	397974.683	-0.046*	143.2321	4.17	11 - 10	2	A+	488126.413	0.020	112.7726	7.17
9 - 8	6	E	397909.896	-0.031	173.8929	3.36	11 - 10	2	A-	485840.596	0.026	112.5222	7.17
9 - 8	7	E	397902.457	0.104*	210.1900	2.41	11 - 10	3	A+	486582.463	0.015	126.0581	6.85
9 - 8	8	E	397847.838	-0.029	255.2835	1.28	11 - 10	3	A-	486693.816	0.011	126.0667	6.85
9 - 8	-1	E	395022.707	0.012	69.3665	5.92	11 - 10	4	A+	486601.503	-0.008	144.4920	6.49
9 - 8	-2	E	398589.637	0.008	78.7496	5.81	11 - 10	4	A-	486599.169	-0.007	144.4919	6.49
9 - 8	-3	E	398186.127	0.002	95.7177	5.40	11 - 10	5	A+	486484.643	-0.036	171.5647	5.94
9 - 8	-4	E	398026.429	-0.025	116.4964	4.84	11 - 10	5	A-	486484.643	-0.054	171.5647	5.94
9 - 8	-5	E	398006.753	-0.010	140.5949	4.21	11 - 10	6	A±	486315.757	-0.098	206.0988	5.20
9 - 8	-6	E	397985.845	0.008	172.1589	3.40	11 - 10	7	A±	486167.551	-0.123	243.9715	3.35
9 - 8	-7	E	397901.270	-0.134*	212.3515	2.40	11 - 10	8	A±	486130.356	0.157	285.6694	3.08
9 - 8	-8	E	397775.204	-0.778*	257.5522	1.26	11 - 10	9	A±	486100.257	0.193	335.3014	2.47
10 - 9	0	A+	440511.360	0.015	80.9738	6.85	11 - 10	10	A±	485975.555	-0.274*	393.2796	
10 - 9	1	A+	435288.842	-0.004	84.3725	6.76	11 - 10	0	E	482973.845	0.011	99.5809	6.79
10 - 9	1	A-	448145.350	0.000	86.7406	6.75	11 - 10	1	E	489859.465	0.009	104.0923	7.34
10 - 9	2	A+	443527.191	-0.007	96.4905	6.47	11 - 10	2	E	488225.039	-0.033	110.4536	7.15
10 - 9	2	A-	441799.058	0.013	96.3163	6.47	11 - 10	3	E	486932.609	-0.004	123.8791	6.94
10 - 9	3	A+	442358.539	0.003	109.8274	6.12	11 - 10	4	E	486579.263	-0.050	146.2181	6.47
10 - 9	3	A-	442427.193	0.003	109.8324	6.12	11 - 10	5	E	486360.230	-0.096	174.2045	5.85
10 - 9	4	A+	442366.235	0.056*	128.2607	5.71	11 - 10	6	E	486266.814	-0.263*	204.8597	5.19
10 - 9	4	A-	442364.930	-0.080*	128.2607	5.71	11 - 10	7	E	486262.503	0.254	241.1564	4.44
10 - 9	5	A+	442271.778	-0.015	155.3373	5.10	11 - 10	8	E	486196.699	-0.069	286.2457	3.51
10 - 9	5	A-	442271.778	-0.022	155.3373	5.10	11 - 10	9	E	486039.420	-0.322*	338.2493	2.43
10 - 9	6	A±	442131.790	-0.091	189.8771	4.30	11 - 10	10	E	485872.679	0.170	393.3271	1.27
10 - 9	7	A±	442005.649	-0.089	227.7547	3.36	11 - 10	-1	E	481453.390	0.020	100.0456	7.09
10 - 9	8	A±	441972.957	0.126	269.4539	2.27	11 - 10	-2	E	486950.772	0.010	109.7636	7.19
10 - 9	9	A±	441942.577	0.206*	319.0868	1.29	11 - 10	-3	E	486698.423	-0.018	126.7105	6.88
10 - 9	0	E	439592.148	0.028	83.4706	6.26	11 - 10	-4	E	486435.763	-0.012	147.4735	6.40
10 - 9	1	E	445057.491	0.012	87.7524	6.66	11 - 10	-5	E	486405.091	0.003	171.5701	5.90
10 - 9	2	E	443449.221	0.003	94.1681	6.46	11 - 10	-6	E	486381.322	0.009	203.1326	5.26
10 - 9	3	E	442621.029	0.005	107.6367	6.20	11 - 10	-7	E	486266.814	0.247*	243.3181	4.42
10 - 9	4	E	442347.909	-0.023	129.9876	5.70	11 - 10	-8	E	486096.990	-0.220	288.5083	3.45
10 - 9	5	E	442171.101	-0.060	157.9813	5.03	11 - 10	-9	E	485995.511	0.217	336.5027	2.43
10 - 9	6	E	442093.022	-0.062	188.6396	4.30	11 - 10	-10	E	485975.555	0.702*	390.7932	1.29

^a Observed minus calculated line frequencies in MHz. Asterisks indicate blended or barely resolved lines that were excluded from the fit.

^b Calculated upper level energies in cm⁻¹. The zero reference energy is taken as the $J = K = 0 A + v_t = 0$ level, calculated to lie 104.8883 cm⁻¹ above the bottom of the torsional barrier.

^c S is the transition strength. Relative line intensities are given by the product of $\mu^2 S$ and the appropriate Boltzmann factor. The dipole moment components were taken as $\mu_a = 0.836$ and $\mu_b = -1.439$ Debye.

^d Ref. [12].

Table 2

Millimeter-wave frequencies, upper level energies (E_u) and line strengths (μ^2S) for ${}^qR_K(J)$ *a*-type *R*-branch transitions in the $v_t = 1$ first excited torsional state of ${}^{13}\text{CH}_3\text{OD}$

$J' - J''$	K	TS	v_{obs} (MHz)	(o-c) ^a	E_u (cm ⁻¹) ^a	μ^2S^c	$J' - J''$	K	TS	v_{obs} (MHz)	(o-c) ^a	E_u (cm ⁻¹) ^b	μ^2S^c
1 - 0	0	A+	44151.09 ^d	0.081	215.9972	0.71	7 - 6	0	A+	309156.170	-0.196	255.7681	4.91
1 - 0	0	E	44144.06 ^d	0.055	181.2842	0.71	7 - 6	1	A+	306837.993	0.018	234.5803	4.94
4 - 3	0	A+	176621.570	-0.162	229.2526	2.80	7 - 6	1	A-	310682.025	0.031	235.0947	4.93
4 - 3	1	A+	175464.453	0.042	208.2553	2.71	7 - 6	2	A+	308525.522	0.030	225.5268	4.29
4 - 3	1	A-	177670.950	0.029	208.4394	2.70	7 - 6	2	A-	308664.368	0.108	225.5372	4.29
4 - 3	2	A+	176397.498	0.020	199.0586	2.00	7 - 6	3	A+	309122.846	0.017	250.5372	3.97
4 - 3	2	A-	176422.483	0.010	199.0598	2.00	7 - 6	3	A-	309134.487	-0.018	250.5379	3.97
4 - 3	3	A+	176579.710	0.044*	224.0257	1.22	7 - 6	4	A+	308753.624	0.019	299.2660	3.07
4 - 3	3	A-	176580.151	-0.074	224.0257	1.22	7 - 6	4	A-	308753.624	0.030	299.2660	3.07
4 - 3	0	E	176531.362	0.031	194.5344	2.83	7 - 6	5	A±	307583.670	0.012	314.1749	1.61
4 - 3	1	E	176487.076	0.020	191.1411	2.59	7 - 6	6	A±	309829.777	0.089	322.2739	1.58
4 - 3	2	E	176561.834	-0.071	221.2797	2.07	7 - 6	0	E	308758.165	-0.003	221.0226	4.95
4 - 3	3	E	176897.324	-0.021	254.8527	1.45	7 - 6	1	E	308717.063	0.008	217.6247	4.74
4 - 3	-1	E	176571.001	-0.087	225.5059	2.53	7 - 6	2	E	309012.880	-0.060	247.7841	4.44
4 - 3	-2	E	176661.196	-0.016	230.3719	2.25	7 - 6	3	E	309015.554	0.012	281.3737	4.57
4 - 3	-3	E	176244.288	0.004	218.3971	1.08	7 - 6	4	E	307731.569	0.024	274.9171	2.36
5 - 4	0	A+	220790.289	-0.174	236.6173	3.51	7 - 6	5	E	309679.923	0.058	287.0368	2.62
5 - 4	1	A+	219286.286	0.029	215.5699	3.46	7 - 6	6	E	308908.156	0.083	333.2542	1.30
5 - 4	1	A-	222041.723	0.013	215.8459	3.46	7 - 6	-1	E	309127.386	-0.065	252.0172	4.61
5 - 4	2	A+	220463.696	0.024	206.4125	2.80	7 - 6	-2	E	308686.022	-0.027	256.8624	4.77
5 - 4	2	A-	220513.547	0.001	206.4154	2.80	7 - 6	-3	E	308248.450	0.003*	244.8418	3.55
5 - 4	3	A+	220746.184	-0.040	231.3890	2.22	7 - 6	-4	E	309501.250	0.053	263.2364	3.36
5 - 4	3	A-	220748.180	0.002	231.3891	2.22	7 - 6	-5	E	308885.939	0.095	313.6347	2.35
5 - 4	4	A+	220563.873	-0.006	280.1389	1.17	7 - 6	-6	E	307617.885	0.011	358.2657	0.86
5 - 4	4	A-	220563.873	-0.005	280.1389	1.17	8 - 7	0	A+	353356.892	-0.201	267.5548	5.61
5 - 4	0	E	220630.717	0.036	201.8938	3.54	8 - 7	1	A+	350557.828	-0.014	246.2737	5.67
5 - 4	1	E	220582.463	0.006	198.4989	3.32	8 - 7	1	A-	354938.292	0.022	246.9341	5.65
5 - 4	2	E	220708.083	-0.102	228.6418	2.90	8 - 7	2	A+	352512.457	0.011	237.2853	5.01
5 - 4	3	E	221011.173	-0.013	262.2248	2.62	8 - 7	2	A-	352719.717	-0.044	237.3027	5.01
5 - 4	4	E	219790.760	0.011	255.8543	0.89	8 - 7	3	A+	353336.722	0.025	262.3233	4.78
5 - 4	-1	E	220739.002	-0.089	232.8690	3.24	8 - 7	3	A-	353360.011	0.047	262.3247	4.78
5 - 4	-2	E	220733.924	-0.011	237.7348	3.14	8 - 7	4	A+	352835.487	0.001	311.0353	3.91
5 - 4	-3	E	220270.314	-0.021*	225.7446	1.98	8 - 7	4	A-	352835.487	0.031	311.0353	3.91
5 - 4	-4	E	220881.784	0.005	244.0676	1.28	8 - 7	5	A±	351498.518	0.021	325.8996	2.31
6 - 5	0	A+	264967.871	-0.208	245.4557	4.21	8 - 7	6	A±	354037.358	0.083	334.0834	3.02
6 - 5	1	A+	263079.246	0.074	224.3453	4.20	8 - 7	7	A±	353089.903	-0.040	373.9206	0.04
6 - 5	1	A-	266380.935	0.013	224.7314	4.20	8 - 7	0	E	352777.530	-0.026	232.7900	5.66
6 - 5	2	A+	264507.821	0.025	215.2355	3.56	8 - 7	1	E	352749.236	-0.025	229.3912	5.45
6 - 5	2	A-	264594.824	-0.001	215.2413	3.56	8 - 7	2	E	353172.721	-0.058	259.5646	5.18
6 - 5	3	A+	264926.583	0.006	240.2260	3.13	8 - 7	3	E	352886.734	0.005	293.1447	5.42
6 - 5	3	A-	264931.772	-0.007	240.2263	3.13	8 - 7	4	E	351706.035	0.038	286.6488	3.02
6 - 5	4	A+	264662.618	0.003	288.9671	2.17	8 - 7	5	E	354090.854	0.080	298.8480	3.74
6 - 5	4	A-	264662.618	0.006	288.9671	2.17	8 - 7	6	E	353035.771	0.095	345.0302	2.44
6 - 5	5	A±	263659.755	0.004	303.9150	0.85	8 - 7	7	E	352589.788	-0.243	410.0357	1.17
6 - 5	0	E	264707.782	0.023	210.7235	4.25	8 - 7	-1	E	353353.202	-0.053	263.8038	5.29
6 - 5	1	E	264660.328	0.038	207.3270	4.04	8 - 7	-2	E	352545.550	-0.017	268.6221	5.54
6 - 5	2	E	264858.213	-0.082	237.4765	3.68	8 - 7	-3	E	352191.904	-0.001	256.5897	4.28
6 - 5	3	E	265054.201	0.001	271.0660	3.64	8 - 7	-4	E	353901.461	0.068	275.0413	4.28
6 - 5	4	E	263759.457	0.015	264.6523	1.65	8 - 7	-5	E	353003.373	0.079	325.4096	3.35
6 - 5	5	E	265325.290	0.060	276.7070	1.40	8 - 7	-6	E	351549.812	0.025	369.9921	1.63
6 - 5	-1	E	264923.490	-0.093	241.7059	3.93	8 - 7	-7	E	353463.8	-0.078*	380.3073	1.49
6 - 5	-2	E	264745.757	-0.026	246.5658	3.98	9 - 8	0	A+	397571.780	-0.215	280.8164	6.31
6 - 5	-3	E	264273.313	0.121	234.5598	2.79	9 - 8	1	A+	394234.356	-0.036	259.4239	6.39
6 - 5	-4	E	265163.631	0.040	252.9125	2.37	9 - 8	1	A-	399143.064	0.031	260.2481	6.37
6 - 5	-5	E	264765.255	0.055	303.3314	1.26	9 - 8	2	A+	396464.444	0.038	250.5100	5.72

Table 2 (continued)

$J' - J''$	K	TS	v_{obs} (MHz)	(o-c) ^a	E_u (cm ⁻¹) ^a	$\mu^2 S^c$	$J' - J''$	K	TS	v_{obs} (MHz)	(o-c) ^a	E_u (cm ⁻¹) ^b	$\mu^2 S^c$
9 - 8	2	A-	396759.128	-0.069	250.5372	5.72	10 - 9	8	E	439802.598	-0.114	464.1806	2.05
9 - 8	3	A+	397569.506	0.072*	275.5848	5.56	10 - 9	9	E	441376.959	0.057	492.7746	1.44
9 - 8	3	A-	397611.938	0.062	275.5876	5.56	10 - 9	-1	E	441878.481	0.015	291.8059	6.62
9 - 8	4	A+	396906.874	0.010	324.2747	4.72	10 - 9	-2	E	439997.886	-0.055	296.5186	7.02
9 - 8	4	A-	396906.874	0.082	324.2747	4.72	10 - 9	-3	E	439968.273	-0.070	284.4779	5.70
9 - 8	5	A \pm	395402.917	0.030	339.0889	2.97	10 - 9	-4	E	442905.312	0.073	303.1031	6.02
9 - 8	6	A \pm	398223.947	0.096	347.3667	4.29	10 - 9	-5	E	441226.788	0.070	353.3738	5.15
9 - 8	7	A \pm	397229.377	-0.043	387.1708	0.59	10 - 9	-6	E	439392.851	0.023	397.8403	3.03
9 - 8	8	A \pm	396932.789	0.156*	457.2232		10 - 9	-7	E	441603.887	-0.012	408.2984	4.02
9 - 8	0	E	396761.643	0.005	246.0245	6.36	10 - 9	-8	E	441440.872	-0.266	441.6290	2.65
9 - 8	1	E	396753.411	-0.027	242.6254	6.15	10 - 9	-9	E	441063.849	0.310	508.8864	1.33
9 - 8	2	E	397338.355	-0.034	272.8184	5.91	11 - 10	0	A+	486050.787	-0.162	311.7662	7.72
9 - 8	3	E	396662.402	0.048	306.3760	6.21	11 - 10	1	A+	481442.548	-0.148	290.0887	7.82
9 - 8	4	E	395681.289	0.032	299.8473	3.67	11 - 10	1	A-	487371.226	0.040	291.2916	7.78
9 - 8	5	E	398560.515	0.078	312.1425	4.79	11 - 10	2	A+	484246.791	0.016	281.3521	7.12
9 - 8	6	E	397162.471	0.088	358.2781	3.49	11 - 10	2	A-	484781.004	-0.143	281.4106	7.12
9 - 8	7	E	396636.766	-0.244	423.2661	2.22	11 - 10	3	A+	486093.813	0.071	306.5367	7.08
9 - 8	8	E	395876.410	-0.090*	449.5103	1.07	11 - 10	3	A-	486210.291	0.167	306.5458	7.08
9 - 8	-1	E	397603.080	-0.018	277.0665	5.95	11 - 10	4	A+	485012.291	-0.067*	355.1621	6.25
9 - 8	-2	E	396317.415	-0.045	281.8418	6.29	11 - 10	4	A-	485012.291	0.244*	355.1620	6.25
9 - 8	-3	E	396099.630	-0.055	269.8022	4.99	11 - 10	5	A \pm	483174.714	0.085	369.8591	4.23
9 - 8	-4	E	398368.899	0.073	288.3294	5.16	11 - 10	6	A \pm	486525.049	0.097	378.3518	6.57
9 - 8	-5	E	397117.166	0.088	338.6560	4.27	11 - 10	7	A \pm	485510.782	-0.125	418.0882	4.66
9 - 8	-6	E	395475.266	0.028	383.1838	2.35	11 - 10	8	A \pm	485089.944	0.020	488.1147	2.88
9 - 8	-7	E	397550.046	-0.032	393.5681	2.81	11 - 10	9	A \pm	483128.185	-0.005	542.9836	
9 - 8	-8	E	397308.488	-0.217	426.9042	1.39	11 - 10	10	A \pm	484919.021	0.884*	571.3626	
10 - 9	0	A+	441802.571	-0.180	295.5533	7.02	11 - 10	0	E	484607.064	-0.132	276.8896	7.77
10 - 9	1	A+	437863.654	-0.110	274.0295	7.11	11 - 10	1	E	484663.865	-0.096	273.4931	7.55
10 - 9	1	A-	443289.582	0.027	275.0347	7.08	11 - 10	2	E	485688.662	0.017	303.7464	7.35
10 - 9	2	A+	440377.212	0.011	265.1994	6.42	11 - 10	3	E	483924.377	0.113	337.2061	7.66
10 - 9	2	A-	440780.291	-0.104	265.2400	6.42	11 - 10	4	E	483626.146	0.118	330.6446	4.95
10 - 9	3	A+	441821.791	0.041	290.3233	6.33	11 - 10	5	E	487669.210	0.115	343.1893	6.76
10 - 9	3	A-	441894.151	0.136	290.3276	6.33	11 - 10	6	E	485412.639	0.148	389.1895	5.40
10 - 9	4	A+	440966.300	-0.010	338.9838	5.49	11 - 10	7	E	484700.714	-0.319	454.1333	4.09
10 - 9	4	A-	440966.300	0.146	338.9838	5.49	11 - 10	8	E	483709.974	-0.110*	480.3154	2.95
10 - 9	5	A \pm	439295.471	0.056	353.7422	3.60	11 - 10	9	E	485388.350	0.226	508.9654	2.75
10 - 9	6	A \pm	442387.220	0.087	362.1231	5.47	11 - 10	10	E	485187.680	-0.359	570.4450	1.37
10 - 9	7	A \pm	441369.682	-0.082	401.8933	3.12	11 - 10	-1	E	486180.149	0.113	308.0232	7.27
10 - 9	8	A \pm	441014.708	0.121	471.9339	2.41	11 - 10	-2	E	483586.962	-0.055	312.6493	7.74
10 - 9	9	A \pm	439243.901	-0.005	526.8682	0.94	11 - 10	-3	E	483794.897	-0.095	300.6156	6.39
10 - 9	0	E	440706.164	-0.050	260.7249	7.07	11 - 10	-4	E	487508.947	0.111	319.3647	6.85
10 - 9	1	E	440726.067	-0.074	257.3265	6.85	11 - 10	-5	E	485331.819	0.095	369.5627	6.00
10 - 9	2	E	441510.225	-0.015*	287.5456	6.63	11 - 10	-6	E	483301.088	0.086	413.9615	3.68
10 - 9	3	E	440340.800	0.072	321.0641	6.95	11 - 10	-7	E	485622.686	0.047	424.4971	5.13
10 - 9	4	E	439655.450	0.083	314.5126	4.32	11 - 10	-8	E	485568.807	-0.289	457.8259	3.81
10 - 9	5	E	443088.178	0.124	326.9224	5.79	11 - 10	-9	E	485150.636	0.190	525.0692	2.54
10 - 9	6	E	441288.135	0.092	372.9979	4.47	11 - 10	-10	E	484058.442	-0.130	604.7657	1.11
10 - 9	7	E	440674.105	-0.286*	437.9654	3.18							

^a Observed minus calculated line frequencies in MHz. Asterisks indicate blended or barely resolved lines that were excluded from the fit.

^b Calculated upper level energies in cm⁻¹. The zero reference energy is taken as the $J = K = 0$ A+ $v_t = 0$ level, calculated to lie 104.8883 cm⁻¹ above the bottom of the torsional barrier.

^c S is the transition strength. Relative line intensities are given by the product of $\mu^2 S$ and the appropriate Boltzmann factor. The dipole moment components were taken as $\mu_a = 0.836$ and $\mu_b = -1.439$ Debye.

Table 3

Millimeter-wave frequencies, upper level energies (E_u) and line strengths ($\mu^2 S$) for ${}^rQ_K(J)$ and ${}^pQ_K(J)$ *b*-type Q -branch transitions in the $v_t = 0$ ground torsional state of ${}^{13}\text{CH}_3\text{OD}$

Table 3 (continued)

J	v_{obs} (MHz)	(o-c) ^a	E_u (cm ⁻¹) ^b	$\mu^2 S^c$	J	v_{obs} (MHz)	(o-c) ^a	E_u (cm ⁻¹) ^b	$\mu^2 S^c$	J	v_{obs} (MHz)	(o-c) ^c	E_u (cm ⁻¹) ^b	$\mu^2 S^c$									
$K = -2 \leftarrow -1 E$																							
2	270973.310	-0.020	16.7212	1.71	18	350952.86	-0.68	237.9323	D	20	378715.734	0.077	321.6851	9.05									
3	271096.615	-0.005	21.1493	3.01	19	362048.19	-0.81	264.3957	D	21	391406.723	0.001	352.5080	10.28									
4	271425.234	0.001	27.0542	4.19	20	373812.25	-0.91	292.3138	D	22	404822.804	0.056	384.7805	11.17									
5	272094.393	0.047	34.4366	5.33	21	386282.59	-1.01	321.6851	D	$K = -3 \leftarrow -2 E$													
6	273261.097	0.076	43.2972	6.44	22	399471.17	-1.02	352.5080	D	3	510101.191	0.077	38.1645	1.76									
7	275089.882	0.101	53.6363	7.50	23	413364.70	-1.03	264.3957	D	4	510032.518	0.001	44.0671	3.18									
8	277731.712	0.120	65.4541	8.52	$K = -2 \leftarrow 0 E$																		
9	281298.656	0.131	78.7496	9.47	11	305267.60	-0.81	109.7636	D	5	509911.900	0.056	51.4454	4.46									
10	285840.905	0.105	93.5207	10.34	12	309988.12	-0.94	127.4739	D	6	509721.208	0.039	60.2996	5.65									
11	291338.278	0.086	109.7636	11.09	13	315456.86	-0.86	146.6476	D	7	509448.099	0.018	70.6297	6.80									
12	297717.740	0.061	127.4739	11.65	14	321708.44	-0.85	167.2816	D	8	509094.938	0.010	82.4357	7.90									
13	304892.609	0.040	146.6476	12.00	15	328806.60	-0.79	189.3743	D	9	508691.427	0.003	95.7177	8.92									
14	312795.241	-0.045	167.2816	12.11	16	336825.71	-0.64	212.9248	D	10	508307.138	-0.038	110.4760	9.79									
15	321382.229	-0.155	189.3743	11.91	17	345828.45		237.9323	D	11	508054.824	-0.032	126.7105	10.45									
16	330621.245	-0.284	212.9248	11.30	18	355840.471	-0.226	264.3957	5.55	12	508072.756	-0.068	144.4214	10.84									
17	340483.13	-0.46	237.9323	d	19	366829.627	-0.112	292.3138	7.43	13	508490.170	-0.102	163.6090	10.99									

^a Observed minus calculated line frequencies in MHz.

^b Calculated upper level energies in cm⁻¹. The zero reference energy is taken as the $J = K = 0 A + v_t = 0$ level, calculated to lie 104.8883 cm⁻¹ above the bottom of the torsional barrier.

^c S is the transition strength. Relative line intensities are given by the product of $\mu^2 S$ and the appropriate Boltzmann factor. The dipole moment components were taken as $\mu_a = 0.836$ and $\mu_b = -1.439$ Debye.

^d For $J \geq 17$, the K -labeling for the strongly mixed $K = 0$ and $-1 E$ $v_t = 0$ levels was interchanged by the computer program and the $J = 17 K = 0 E$ level was missing. Thus, the line strengths were not calculated for Q -branch lines with $J \geq 17$ for $K = -2 \leftarrow -1$ and with $J \leq 17$ for $K = -2 \leftarrow 0$. These transitions were not included in the fit but were located later.

Table 4

Millimeter-wave frequencies, upper level energies (E_u) and line strengths (μ^2S) for ${}^rQ_K(J)$ and ${}^pQ_K(J)$ *b*-type Q -branch transitions in the $v_t = 1$ first excited torsional state of $^{13}\text{CH}_3\text{OD}$

J	v_{obs} (MHz)	(o-c) ^a	E_u (cm ⁻¹) ^b	μ^2S^c	J	v_{obs} (MHz)	(o-c) ^a	E_u (cm ⁻¹) ^b	μ^2S^c	J	v_{obs} (MHz)	(o-c) ^c	E_u (cm ⁻¹) ^b	μ^2S^c									
$K = 1A^+ \leftarrow 2A^-$																							
2	277336.221	-0.022	198.0121	1.58	10	442445.402	0.043*	353.7422	4.93	22	304987.539	-0.165	653.7402	14.24									
3	276631.757	0.026	202.4025	2.73	11	440607.841	0.212*	369.8591	5.51	23	310545.176	-0.177	687.5520	14.66									
4	275673.717	0.048	208.2553	3.74	12	438603.041	-0.123	387.4393	6.05	24	316249.855	-0.162	722.8215	15.08									
5	274446.456	0.076	215.5699	4.67	13	436431.983	-0.092	406.4820	6.56	25	322107.973	0.243	759.5474	15.50									
6	272930.823	0.096	224.3453	5.53	14	434094.402	-0.079	426.9868	7.02														
7	271104.559	0.117	234.5803	6.32	15	431590.395	-0.108	448.9529	7.45	$K = 5A^- \leftarrow 4A^+, \text{cont'd}$													
8	268942.645	0.122	246.2737	7.04	16	428920.192	-0.069	472.3797	7.84	16 ^d	274784.862	-0.137	481.5455	11.40									
9	266417.872	0.154	259.4239	7.69	17	426083.786	-0.072	497.2664	8.20	17	279417.144	-0.241	506.5867	11.95									
10	263501.239	0.152	274.0295	8.27	18	423081.284	-0.089	523.6121	8.52	18	284220.973	-0.386	533.0927	12.45									
11	260162.743	0.108	290.0887	8.77	19	419912.748	-0.098	551.4160	8.81	19	289187.396	-0.090	561.0623	12.93									
12	256372.077	0.058	307.5997	9.21	20	416578.107	-0.156	580.6771	9.07	20	294307.943	-0.131	590.4942	13.38									
13	252099.285	-0.003	326.5608	9.56	21	413077.340	-0.202	611.3945	9.30	21	299577.435	-0.123	621.3873	13.82									
14	247315.596	-0.071	346.9701	9.85	22	409410.250	-0.267	643.5669	9.49	22	304992.855	-0.046	653.7404	14.24									
15	241994.185	-0.134	368.8257	10.06	23	405576.438	-0.480	677.1934	9.66	23	310554.020	0.016	687.5523	14.66									
16	236110.893	-0.199	392.1257	10.21	24	401575.892	-0.469	712.2726	9.79	24	316264.236	0.112	722.8220	15.08									
17	229644.945	-0.241	416.8682	10.29	25	397407.729	-0.601	748.8032	9.89	25	322130.475	0.182	759.5483	15.51									
18	222579.480	-0.250	443.0516	10.32	$K = 5A^+ \leftarrow 4A^-$																		
19	214902.014	-0.224	470.6741	10.29	5	449130.007	-0.026	295.1203	1.10	4	189763.612	0.049	254.8527	1.39									
20	206604.840	-0.087	499.7341	10.22	6	448127.146	-0.026	303.9150	2.05	5	190984.038	0.039	262.2248	2.41									
21	197684.949	0.061	530.2300	10.11	7	446957.179	-0.057	314.1749	2.88	6	192278.787	0.029	271.0660	3.17									
22	188144.491	0.377	562.1604	9.97	8	445620.211	-0.065	325.8996	3.62	7	193562.755	0.001	281.3737	3.73									
23	177990.204	0.795	595.5240	9.80	9	444116.231	-0.140	339.0889	4.30	8	194743.501	0.016	293.1447	4.11									
24	167233.677	0.042	630.3196	9.59	10	442445.402	-0.229*	353.7422	4.93	9	195724.570	-0.012	306.3760	4.33									
25	155887.090	-0.416	666.5458	9.40	11	440607.841	-0.372*	369.8591	5.51	10	196409.920	-0.023	321.0641	4.41									
$K = 1A^- \leftarrow 2A^+$																							
2	278995.380	-0.019	198.0674	1.57	12	438604.279	-0.052	387.4393	6.05	11	196708.163	-0.016	337.2061	4.37									
3	279956.786	-0.034	202.5130	2.71	13	436434.204	-0.070	406.4820	6.56	12	196536.941	0.002	354.7989	4.23									
4	281230.232	-0.032	208.4394	3.69	14	434098.345	-0.086	426.9868	7.02	13	195826.599	0.021	373.8400	4.02									
5	282808.303	0.001	215.8459	4.56	15	431597.266	-0.045	448.9529	7.45	14	194522.702	0.030	394.3271	3.76									
6	284681.420	-0.008	224.7314	5.35	16	428931.518	-0.058	472.3797	7.84	15	192587.146	0.065	416.2584	3.48									
7	286837.932	0.002	235.0947	6.03	17	426102.057	-0.024	497.2664	8.20	16	189997.639	0.087	439.6327	3.19									
8	289263.767	0.013	246.9341	6.62	18	423109.984	0.076	523.6121	8.52	17	186746.238	0.093*	464.4490	2.91									
9	291942.398	0.017	260.2481	7.11	19	419956.437	0.010	551.4160	8.81	18	182836.992	0.098*	490.7066	2.65									
10	294854.758	0.023	275.0347	7.48	20	416643.409	0.063	580.6771	9.07	19	178283.299	0.113	518.4052	2.41									
11	297979.183	0.038	291.2916	7.73	21	413172.854	0.075	611.3945	9.30	20	173105.288	0.078	547.5445	2.19									
12	301291.440	0.040	309.0166	7.87	22	409547.460	0.138	643.5669	9.49	21	167327.772	0.056	578.1243	2.00									
13	304764.977	0.060	328.2070	7.89	23	405770.350	0.214	677.1933	9.66	22	160978.207	0.025	610.1444	1.84									
14	308371.140	0.066	348.8601	7.80	24	401845.412	0.374	712.2725	9.79	23	154085.295	-0.098	643.6047	1.71									
15	312079.768	0.046	370.9729	7.59	25	397777.245	0.648	748.8031	9.89	$K = 5 \leftarrow 4E$													
16	315859.926	0.034	394.5425	7.28	6	240556.900	-0.222	311.9391	1.79	6	361389.807	-0.130	276.7070	3.55									
17	319680.721	0.010	419.5656	6.88	7	242803.110	-0.051	322.2739	3.36	7	363338.183	-0.073	287.0368	5.13									
18	323512.467	-0.016	446.0390	6.40	8	245341.857	-0.083	334.0834	4.69	8	365723.002	-0.031	298.8480	6.67									
19	327327.865	-0.011	473.9597	5.85	9	248162.870	-0.034	347.3667	5.87	9	368602.209	-0.003	312.1425	8.20									
20	331103.093	-0.048	503.3246	5.26	10	251254.638	0.016	362.1231	6.92	10	372034.917	0.017	326.9224	9.75									
21	334819.167	-0.078	534.1307	4.65	11	254604.971	0.026	378.3518	7.86	11	376078.002	0.035	343.1893	11.30									
22	338462.770	-0.038	566.3753	4.03	12	258201.232	0.045	396.0519	8.71	12	380782.577	0.022	360.9447	12.86									
23	342026.736	-0.002	600.0558	3.41	13	262030.352	0.020	415.2224	9.48	13	386191.031	0.014	380.1899	14.42									
24	345510.545	0.053	635.1700	2.83	14	266079.246	-0.016	435.8622	10.18	14	392334.825	0.009	400.9254	15.98									
25	348920.130	0.190	671.7157	2.28	15	270334.949	-0.030	457.9703	10.82	15	399233.665	-0.036	423.1514	17.51									
$K = 5A^- \leftarrow 4A^+$																							
5	449130.007	-0.026	295.1203	1.10	16	274784.862	0.003	481.5455	11.40	16	406896.139	-0.045	446.8676	19.03									
6	448127.146	-0.022	303.9150	2.05	17	279417.144	0.036*	506.5867	11.95	17	415321.022	-0.073	472.0734	20.51									
7	446957.179	-0.042	314.1749	2.88	18	284220.973	0.143*	533.0927	12.45	18	424499.686	-0.087	498.7676	21.96									
8	445620.211	-0.020	325.8996	3.62	19	289186.299	-0.210	561.0622	12.93	19	434418.375	-0.095	526.9490	23.39									
9	444116.231	-0.023	339.0889	4.30	20	294306.148	-0.176	590.4941	13.38	20	445060.509	-0.098	556.6160	24.78									
					21	299574.333	-0.173	621.3872	13.82	21	456408.584	-0.053	587.7670	26.16									

Table 4 (continued)

<i>J</i>	v _{obs} (MHz)	(o-c) ^a	<i>E_u</i> (cm ⁻¹) ^b	μ^2S^c	<i>J</i>	v _{obs} (MHz)	(o-c) ^a	<i>E_u</i> (cm ⁻¹) ^b	μ^2S^c	<i>J</i>	v _{obs} (MHz)	(o-c) ^c	<i>E_u</i> (cm ⁻¹) ^b	μ^2S^c
<u><i>K = 5 ← 4 E, cont'd</i></u>					<u><i>K = -2 ← -3 E, cont'd</i></u>					<u><i>K = -7 ← -6 E, cont'd</i></u>				
22	468445.364	-0.079	620.4004	27.51	13	359471.092	0.043	349.2613	3.97	12	318253.118	-0.133	442.1627	7.23
23	481155.219	-0.027	654.5146	28.86	14	358335.117	0.094	369.7378	3.44	13	320716.169	-0.122	461.2941	8.01
24	494524.107	0.039	690.1078	30.19	15	356860.223	0.185	391.6588	2.87	14	323209.566	-0.149	481.8899	8.71
25	508539.887	0.063	727.1785	31.52	16	355058.135	0.208	415.0232	2.31	15	325706.814	-0.111	503.9485	9.33
<u><i>K = -2 ← -3 E,</i></u>					17	352959.674	0.215	439.8306	1.78	16	328181.849	-0.096	527.4685	9.89
3	358577.961	0.019	224.4791	1.58	18	350618.503	0.135	466.0815	1.28	17	330609.679	-0.062	552.4483	10.39
4	358994.904	0.035	230.3719	2.73	19	348120.980	-0.085	493.7775	0.85	18	332966.497	-0.011	578.8863	10.84
5	359458.495	0.026	237.7348	3.61	20	345610.011	-0.565	522.9221	0.48	19	335229.954	0.008	606.7809	11.24
6	359931.048	-0.012	246.5658	4.28	21	343345.016	-1.600*	553.5230	0.19	20	337379.679	0.155	636.1304	11.60
7	360368.660	-0.002	256.8624	4.75	<u><i>K = -7 ← -6 E</i></u>					21	339396.805	0.092	666.9333	11.91
8	360722.317	-0.007	268.6221	5.03	7	307325.930	0.081	368.5170	1.66	22	341265.312	0.104	699.1877	12.19
9	360940.086	-0.013	281.8418	5.12	8	309239.962	0.022	380.3073	3.07	23	342971.165	0.041	732.8921	12.44
10	360969.692	-0.005	296.5186	5.04	9	311314.741	-0.039	393.5681	4.31	24	344503.061	-0.117	768.0448	12.66
11	360761.723	0.000	312.6493	4.80	10	313525.783	-0.068	408.2984	5.40	25	345852.502	-0.334	804.6440	12.84
12	360273.241	0.036	330.2311	4.43	11	315847.381	-0.108	424.4971	6.37					

^a Observed minus calculated line frequencies in MHz. Asterisks indicate blended lines or lines with large residuals that were excluded from the fit.

^b Calculated upper level energies in cm⁻¹. The zero reference energy is taken as the *J = K = 0 A + v_t = 0* level, calculated to lie 104.8883 cm⁻¹ above the bottom of the torsional barrier.

^c *S* is the transition strength. Relative line intensities are given by the product of μ^2S and the appropriate Boltzmann factor. The dipole moment components were taken as $\mu_a = 0.836$ and $\mu_b = -1.439$ Debye.

^d The *J = 6 to 15 A⁺ ← A⁻* components for the *K = 6 ← 5 A v_t = 1 Q*-branch are not listed separately since the *K*-type doubling is not resolved and the (o-c) values for the two components differ by less than 0.1 MHz.

Table 5

Principal fitted molecular parameters (in cm^{-1}) for $^{13}\text{CH}_3\text{OD}$ and comparison to related methanol isotopologues

Param	$^{13}\text{CH}_3\text{OD}$	CH_3OD	CH_3OH	$^{13}\text{CH}_3\text{OH}$
<i>A</i>	3.675259(77)	3.673981(5)	4.2537233(71)	4.2538428(51)
<i>B</i>	0.7624739(18)	0.7823356(4)	0.8236523(70)	0.8034196(51)
<i>C</i>	0.71537708(83)	0.7328606(4)	0.7925575(71)	0.7737925(50)
<i>F</i>	17.41869(15)	17.42806(1)	27.6468464(28)	27.64201624(70)
ρ^{a}	0.6959(17)	0.6993443(2)	0.8102062230(37)	0.8101648121(45)
V_3	366.034(37)	366.3400(1)	373.544746(12)	373.741301(27)
D_{ab}	0.0268334(83)	0.028047(3)	-0.0038095(38)	-0.0043475(87)

^a Dimensionless.